Starter/Generator Employing Resonant-Converter-fed Induction Machine Part II: Hardware Prototype

IRFAN ALAN, Member, IEEE
Ege University

THOMAS A. LIPO, Fellow, IEEE
University of Wisconsin

Feasibility of operation of a new procedure to start a jet engine (JE) and to generate power by means of a single induction machine (IM) directly coupled to the turbine has been shown by means of a hardware prototype. An introduction, background, operation principle of this type of a system and software simulation portion was presented in Part I of this article. Both in software simulation and in the experimental phase of the studies the JE is replaced by a dc machine. The dc machine is brought to an initial speed by the motoring operation of the IM. Later, the IM is taken into generating mode and the dc machine is into motoring mode of operation. This mode would correspond to the turbine catch-up initiation phase and initiate driving phase of the induction generator (IG) in the actual world. The generated power is then converted to a three-phase 3Ø, 400 Hz (in software), 60 Hz (in hardware), 115 V voltage-regulated bus via a double stage power conversion utilizing a 20 kHz parallel resonant high frequency (HF) ac link and pulse density modulated (PDM) converter technology. Independent of the coupled machine speed, a constant amplitude and constant frequency 3Ø voltage-regulated ac bus is formed and maintained by the proper control of the power converters.

Manuscript received September 29, 1998; revised March 20, 2000; released for publication June 2, 2000.

IEEE Log No. T-AES/36/4/11377.

Refereeing of this contribution was handled by W. M. Polivka.

Authors' addresses: I. Alan, Dept. of Electrical Engineering, Ege University, Bornova, Izmir, Turkey 35100, E-mail: (irfanal@alpha.eng.ege.edu.tr); T. A. Lipo, Dept. of Electrical and Computer Engineering, University of Wisconsin, 1415 Engineering Dr., Madison, WI 53706-1607, E-mail: (lipo@eceserv0.ece.wisc.edu).

I. INTRODUCTION AND BACKGROUND

A detailed introduction and background sections are presented in the Part I of this article [1–44].

Here, the feasibility of operation of the system whose software simulations are presented in Part I has been shown experimentally in a hardware prototype. The hardware configuration, the control strategy, the test of operation of the system, and the evaluation of the test results are presented here. The principal motivation for this phase of the work is to show the feasibility of operation of the entire system by means of an experimental set-up. The power circuit layout of the experimantal system is illustrated in Fig. 1. A secondary motivation has been to provide a basis for a possible industrial implementation.

An existing complete double bridge (3Ø pulse density modulated (PDM)) ac link system constructed for the earlier studies at the University of Wisconsin [37–41] is utilized for the hardware prototype of this study.

II. DESCRIPTION OF THE LABORATORY SYSTEM

For the full scale hardware test a 3Ø/60 Hz, 30 Hp Marathon Electric induction machine (IM) available in the laboratory is chosen. A complete open circuit, blocked rotor and load tests are carried out and additional data is obtained from the manufacturer to establish reliable equivalent circuit parameters. The nameplate ratings and equivalent circuit parameters for this machine are given in Appendix A. Since the jet engine (JE) turbine is replaced by a dc machine for the laboratory prototype and the available dc machines in the lab cannot be operated at high speeds, the 3Ø/300 Hz, 10 Hp Reuland Electric IM which is used in the previous studies [37–40] is not chosen for the hardware test. The nameplate ratings and equivalent circuit parameters of the dc machine, used to replace the JE turbine, are given in Appendix B.

Three-phase 60 Hz utility bus voltage available in the laboratory is used as reference for establishing and maintaining the desired bus in the experimental design, construction, and test phase. Therefore the feasibility of the system in terms of the experimental phase has been demonstrated at 60 Hz even though the simulations carried out were at 400 Hz. The reason for the selection of 60 Hz instead of 400 Hz for the experimental phase was due to the synchronization studies of the established bus with the existing bus. Therefore, in the lab the existing 3Ø 60 Hz bus was convenient for this purpose.

One of the existing 3Ø PDM bridges is used for the IM operating from the 20 kHz high frequency (HF) ac link and the other is used to establish the 3Ø voltage regulated bus. A single-phase bidirectional full-bridge PDM converter for the battery starter interface was constructed as an extension to the

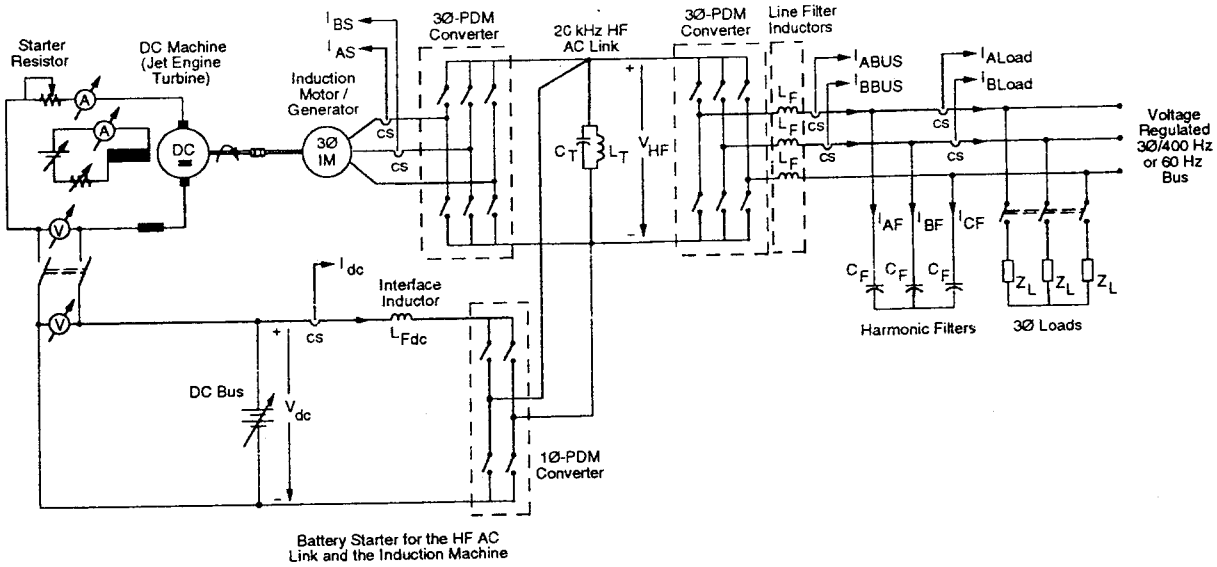

Fig. 1. Power circuit block diagram of battery started and IG maintained 3Ø/400 Hz bus utilizing 20 kHz parallel resonant HF ac link and pulse density modulation technology.

existing complete double bridges. This new 1Ø PDM bridge was designed and built to handle the IM start-up as a motor. The overall power circuit layout of the system including the existing 3Ø PDM double bridges as well as battery starter 1Ø PDM bridge is shown in Fig. 1.

Each switch used in the existing 3Ø PDM double bridges has been constructed from a single insulated gate bipolar transistor (IGBT) and a diode bridge around it [37–41]. However, each switch used in the 1Ø PDM bridge has been constructed by using two IGBTs and two anti-parallel diodes. The components used in the power circuit of the system are listed in detail in [37–41].

The control block diagram for maintaining the average active power balance in the overall system during both motoring and generating mode of operation of IM is given in Part I of this article.

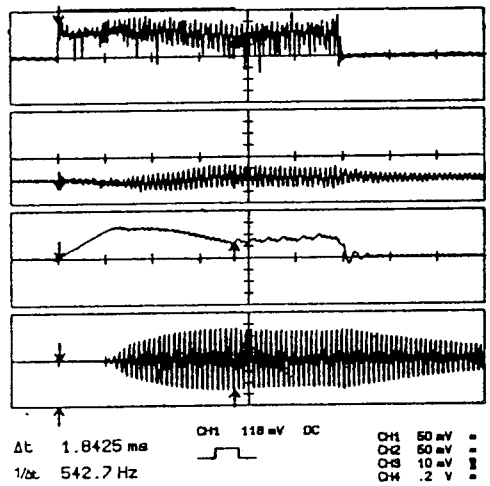

Fig. 2. Test start of link voltage build-up and regulation of HF peak link voltage by battery starter. i^*_{dc}: Battery starter current reference, 5A/div. $-i^*_{dc}$: Estimated negative battery starter current reference, 5A/div. i_{dc}: Battery starter current, 5A/div. $V_{HF\ Link}$: HF link voltage, 200 V/div. Time/div: 0.5 ms.

III. TEST START OF THE BATTERY STARTER

As a first step, the operation of 1Ø PDM converter and the link voltage build-up by means of the battery starter was verified. In this test the 3Ø PDM converters are not engaged. Therefore, neither the IM nor the 3Ø/60 Hz bus is operational at this point.

Fig. 2 shows the HF ac link voltage build-up by the battery starter. Depending upon the average active power need of the operational portion of the system and the operating voltage level of the battery, a dc current reference is estimated for the battery starter. A signal from a minor proportional-integral (PI) peak link voltage regulator contributes to the estimation to compansate for the sudden peak link voltage variations. The resulting sum of these two signals results in the dc current reference for the battery starter. This current is regulated via 1Ø PDM converter to build-up and maintain the HF ac link voltage across the resonant tank circuit elements. Operation of the circuit is simple, and it is a boost type of converter. Initially some energy is stored on the battery side interface inductor, and later this energy is delivered to the HF ac link by turning on appropriate switches in the converter while the actual current is regulated around its reference. The reference current is regulated in this manner with a possibility of switching to a different switch combination at every zero crossing of the 20 kHz HF ac link voltage, i.e., every 25 μs.

In the test corresponding to Fig. 2 the battery or dc bus voltage was set at 120 V and two of the

resonant tank circuit elements which are sufficient to operate the entire system at about 7 kW power level were connected to the link. The top trace in Fig. 2 shows the time of application and removal of the reference current to 1Ø PDM converter. The ringing seen in the reference current is due to the minor PI peak link voltage regulator contribution. After the dc current reference is applied there seems to be no activity in the HF ac link voltage for about 500 μs though the actual current continues to rise at this time period. This fact is due to the energy storage period of the interface inductor. Through this period there is no energy delivered to the link. Later, when the actual current reaches its reference, the stored energy is delivered to the HF link and the voltage begins building up. A zero current reference is also well regulated revealing zero active power delivery to the link. When a zero current reference is applied while the link voltage is established, the link voltage starts to die out depending on its quality factor Q. Having a battery starter voltage of 120 V, Fig. 2 reveals that a 960 W average active power is sufficient to keep the HF link peak at around 500 V with all the losses of the HF link and the 1Ø PDM converter.

IV. EXCITATION AND MOTORING OPERATION OF INDUCTION MACHINE

After verifying correct operation of the 1Ø PDM converter, the IM side 3Ø PDM converter was given a test start for short periods of time. Fig. 3 shows such a test start for a period of 1.65 ms. Before the 3Ø PDM converter was enabled, the link voltage was established and regulated by means of 1Ø PDM converter and the battery. As soon as the 3Ø PDM converter is enabled, the actual phase-A line current of IM follows its applied reference as seen from the top two traces on top of each other in the figure. The enable signal for the associated 3Ø PDM converter is displayed on the bottom trace together with the HF ac link voltage. During the start up of excitation procedure the peak of the link voltage experiences a transient. When the operation of the 3Ø PDM converter is disabled, the actual current returns to zero within roughly 500 μs. However, the link voltage remains regulated due to the continued operation of the single-phase PDM converter and the battery starter.

Fig. 4 shows the same procedure, this time with a much longer test period time. In this figure the associated 3Ø PDM converter is enabled for about 1.27 s. During the excitation period, roughly the open circuit rotor time constant, only a command corresponding to the rated flux component of current is applied to the IM. About 670 ms later, as can be noticed from the figure a jump in the line current and its reference is observed. This jump in the current

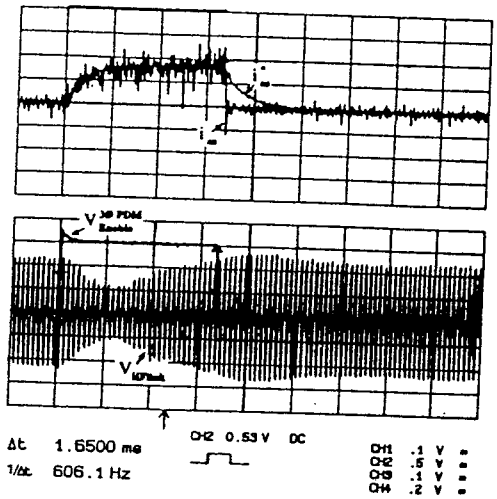

Fig. 3. Test start and operation of 3Ø-PDM converter and excitation of IM for 1.65 ms. i_{as}^{*} and i_{as}: Phase-A IM reference and measured currents, 10 A/div. $V_{\text{Enable}}^{3\text{Ø-PDM}}$: IM side 3Ø-PDM converter enable signal, 5 V/div. $V_{\text{HF Link}}$: HF link voltage, 200 V/div. Time/div: 0.5 μs.

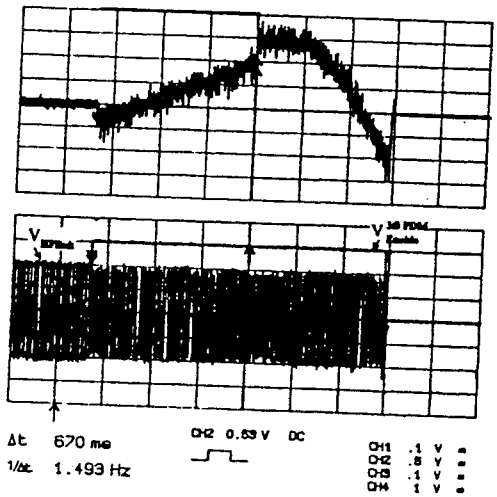

Fig. 4. Test start of excitation and motoring mode of operation of the IM. i_{as}^{*} and i_{as}: Phase-A induction reference and measured currents, 10 A/div. $V_{\text{Enable}}^{3\text{Ø-PDM}}$: IM side 3Ø-PDM converter enable signal, 5 V/div. $V_{\text{HF Link}}$: HF link voltage, 200 V/div. Time/div: 0.2 s.

signifies that the IM is applied its torque component current command in addition to its flux component. The machine from this point on is now test started for motoring operation for about 0.6 s. At the end of the test period everything is disabled.

V. INDUCTION MACHINE IN MOTORING AND SPEED REGULATION MODE

After verifying a reliable start of the IM in the motoring mode, speed regulation in motoring mode is tested. During these tests the dc machine is mechanically coupled to the IM and initially behaves as an additional inertia to the system. Thus, as the

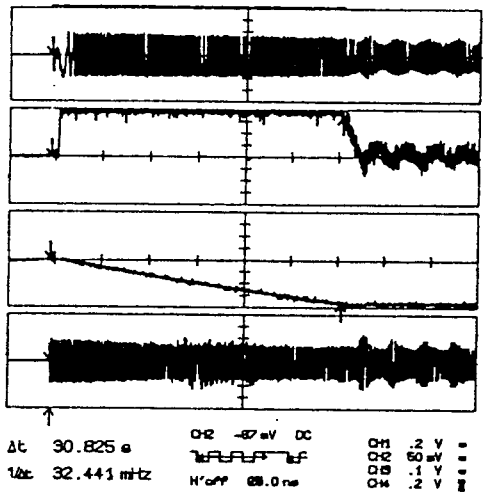

Fig. 5. General view of start and test of operation of IM in motoring and speed regulation mode. i^*_{as}: Phase-A IM current reference, 20 A/div. i_{qsref}: Torque component current command of IM, 5 A/div. Speed: Speed of IMO, 667 r/min/div. $V_{HF\ Link}$: HF link voltage, 200 V/div. Time/div: 5 s.

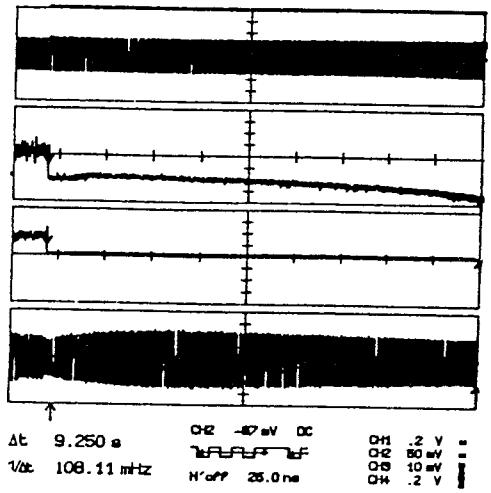

Fig. 6. General view of switching from motoring mode to generating mode of operation of IM i^*_{as}: Phase-A IM current reference, 20 A/div. i_{qsref}: Torque component current command of IM, 5 A/div. i_{dc}: Battery starter current, 10 A/div. $V_{HF\ Link}$: HF link voltage, 200 V/div. Time/div: 1 s.

speed of the IM is regulated, so is the speed of the dc machine.

Fig. 5 shows a view of the start of the link voltage build-up, excitation, and motoring operation of IM. During this operation the battery starter voltage is set at 151 V and the desired speed is set at around 2450 r/min. It takes for the induction motor to speed up to this desired speed about 30.82 s as shown in the figure. Since a limited positive torque component current command is applied to the motor due to the limited power rating of the single-phase PDM converter, the time to reach the desired speed takes long. Even though the rated torque component current command of induction machine is 92.627 A peak, only around 20 A peak maximum is applied during motoring as seen in the second trace. When the desired speed is reached the torque command is reduced by the PI speed regulator to regulate the speed, yet it experiences some oscilations due to the need of gain adjustments of the PI speed regulator. The speed of the machine is shown in the third trace from the top. The last trace in the figure shows the HF ac link voltage. As seen from the figure the peak of link voltage experiences some oscilations during and due to the regulation of the speed.

VI. INDUCTION MACHINE IN GENERATING MODE

Fig. 6 shows the start of operation of the generator with a transition from the motoring mode of operation while disabling and disconnection of the battery starter. The first trace from the top shows the IM phase-A line current reference and the second trace shows the IM torque component current command. While the torque command of the machine has a little positive value during the speed regulation in motoring mode, the torque command takes a nagative value as soon as the generator mode of operation is commanded. This new value of the torque command is estimated in a way to maintain the average active power balance in the entire system depending on the speed of the generator while the battery starter is disconnected in the transition. Since the dc motor coupled to the generator is not activated the speed of the generator starts to die out as the mechanically stored energy is extracted from the generator. Therefore, the torque component current command of the generator is increased to deliver the same amount of active power to the system to maintain the operation. The last trace shows the HF link voltage before, during, and after the transition from the motoring to the generating mode of operation.

Fig. 7 shows an entire cycle of a starting procedure where the link voltage is built up, the IM is excited, the motoring and speed regulation mode and thereafter a generating mode of operation is commanded. As seen from the figure it takes about 35 s for the motor to reach the desired speed of around 2400 r/min. The speed of the machine is shown in the third trace from the top. During this operation the battery starter voltage is set at 230 V. One can deduce from the first and the third traces from the top that just before reaching the desired speed in motoring and speed regulation mode the dc current of the battery starter reaches a maximum of around 25–30 A. This means an average active power delivery of around 5.57–6.9 kW from the battery starter to the system. If the desired speed level is increased the peak of this power would also increase. If a lower value of battery starter voltage is chosen, such as 120 V for the same amount of power delivery, this would mean almost twice the battery starter current that would

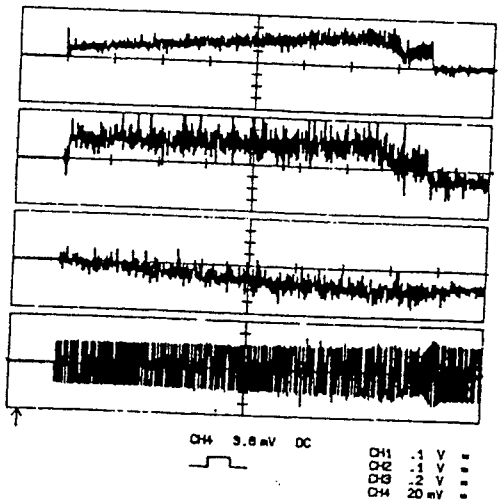

Fig. 7. General view of start of operation, link voltage build-up, excitation of IM, motoring and speed regulation mode by battery starter, switching to generating mode, disconnection of battery starter and operating generator as source of the system. i_{dc}: Battery starter current, 10 A/div. i_{qsref}: Torque component current command of IM, 10 A/div. Speed: Speed of IMO, 1333 r/min/div. $V_{HF\ Link}$: HF link voltage, 200 V/div. Time/div: 5 s.

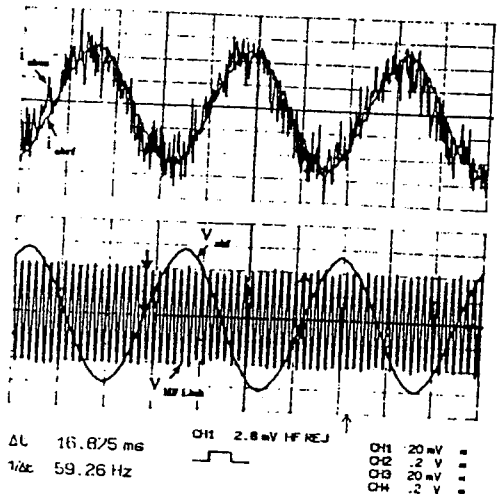

Fig. 8. Start and operation of 3Ø/60 Hz voltage source bus at no load with an 80 V line-line rms utility reference. i_{abus} and i_{abrf}: Phase-A bus current and its reference, 2 A/div. V_{abf}: Phase-AB line to line filtered bus voltage, 40 V/div. $V_{HF\ Link}$: HF link voltage, 200 V/div. Time/div: 5 ms.

be close to the power ratings of the switches used in the single-phase converter. For a safer operation of the converters the battery starter voltage is set at a higher value, and the limit of the torque command of the motor is kept low. The last trace in Fig. 7 shows the HF ac link voltage. As seen from the figure the peak of link voltage goes through some transition right after the transition from motoring mode to the generating mode of operation.

VII. THE ESTABLISHING AND MAINTAINING 3Ø/60 HZ BUS VIA A DEDICATED 3Ø PDM CONVERTER

The principles of establishing the 3Ø/60 Hz bus by means of regulating the filter capacitor and the bus currents were explained in detail in Part I of this article. Initially a 15 μF filter capacitor per phase is used as was simulated for the 400 Hz bus case. However, for a rated voltage value of 115 V rms line to neutral the required peak capacitor current at 60 Hz was so small that the noise superimposed on the capacitor current references made the reference capacitor currents almost indistinguishable from the noise. Therefore, it became necessary to increase the value of the filter capacitor to around 194 μF per phase which is almost an order of magnitude increase for the proper operation of the system.

A. Performance of the 3Ø/60 Hz Bus at No Load

Fig. 8 shows the operation of an unloaded 3Ø/60 Hz bus for nearly 80 V line-to-line rms reference. As seen from the top two traces in the figure the peak of the phase-A bus current reference which in this case is also phase-A filter capacitor current reference is approximately 0.5 V pk signal corresponding to 5 A pk real. Since the amplitude of this signal is quite small the induced noise in the signal has some significant share. This value is even after resizing and increasing the value of the filter cap value to 194 μF per phase. It is possible to further double the current value without doubling the size of the capacitor to reduce the share of the noise in the signal by changing the Amps/Turn ratio of the LEM current sensors in the power circuit. However, this option has also limititations since for loaded operation cases the peak of the bus current would be doubled and it would reduce the peak limit of the bus currents that could be measured and cause increased protection errors due to induced noise in the signals. As seen from the top two traces where both currents are shown on top of each other the actual current has a leading phase shift with respect to its reference. One of the two traces at the bottom shows the line-to-line filtered bus voltage obtained via the application and regulation of the reference bus currents. The other trace at the bottom shows the peak of the HF link voltage. Peak of this voltage does not experience significant problems in amplitude variation since the case is an unloaded one and the average active power that the bus draws from the system is quite low.

Fig. 9 shows a different view of operation of the 3Ø/60 Hz bus at no load. The reference bus voltage in this case is about 115 V line-to-line rms or 162.63 V line-to-line peak as illustrated by phase-AB line-to-line voltage displayed in the last trace from the top. The filtered and measured phase-AB line-to-line bus voltage is displayed in the second trace from the top. The third trace from the top shows the phase-AB

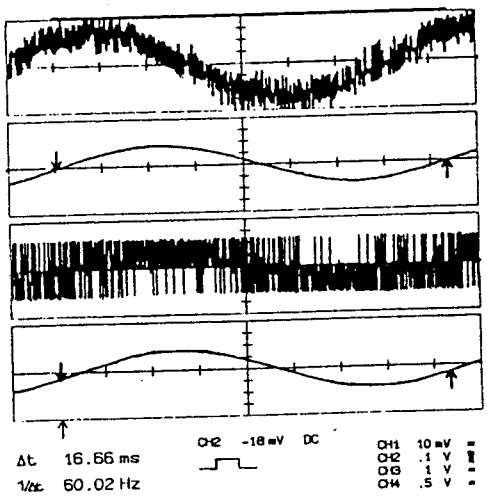

Fig. 9. Another view of operation of 3Ø/60 Hz voltage source bus at no load. i_{abus}: Phase-A bus current, 5 A/div. V_{abf}: Phase-AB line-to-line filtered bus voltage, 100 V/div. V_{abbus}: Phase-AB line-to-line unfiltered bus voltage, 200 V/div. V_{abbrf}: Phase-AB line-to-line bus voltage reference (utility), 100 V/div. Time/div: 2 ms.

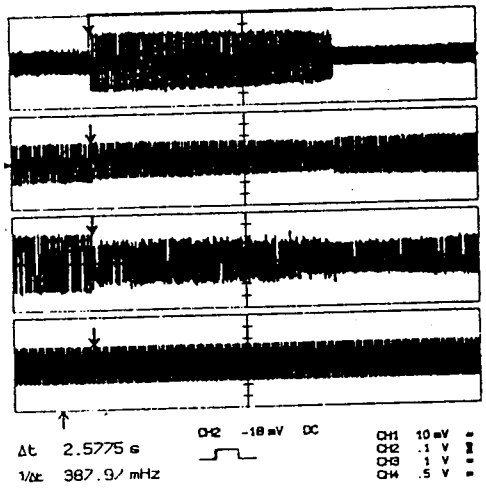

Fig. 10. Response of 3Ø/60 Hz voltage source bus to load variations. i_{abus}: Phase-A bus current, 20 A/div. V_{abf}: Phase-AB line-to-line filtered bus voltage, 100 V/div. V_{abbus}: Phase-AB line-to-line unfiltered bus voltage, 200 V/div. V_{abbrf}: Phase-AB line-to-line bus voltage reference (utility), 100 V/div. Time/div: 2 ms.

line-to-line unfiltered synthesized bus voltage before the interface inductor. This voltage also reflects the peaks of the HF ac link voltage during operation. If carefully examined it can be seen that the filtered bus voltage is leading its reference by several degrees. The basic reason for this leading phase shift is due to the leading phase shift of the regulated actual current with respect to its reference and the nature of the bang bang current regulation technique.

B. The Performance of the 3Ø/60 Hz Bus at Load

Fig. 10 shows the response of the system to a transition from the no load operation of the 3Ø/60 Hz bus to a loaded operation. Initially the bus is operated at no-load and at the middle of the trace sudden step load is applied to the bus. This load is a resistive and balanced 3Ø load. The first trace from the top shows the phase-A bus current. The transition to loading of the bus is very clear from this trace. During the loaded operation of the bus, the line-to-line unfiltered bus voltage peak and the HF peak link voltage are somewhat reduced. The reason for this effect could be the insufficent average active power delivery from the generator to the system.

It is possible to reduce the magnitude of the filtered bus voltage during the operation if desired by simply adjusting the modulation index for the applied voltage reference. Up to now the results were obtained for a modulation index coefficient of 1.0 corresponding to a one-to-one ratio between the reference and the filtered output voltage. Depending upon the magnitude of the desired bus voltage, the modulation index can be adjusted so as to match the desired peak of the bus voltage during the operation.

C. Harmonics and Quality of the Bus Waveforms

Three major waveforms must be examined related to the operation of the established 3Ø/60 Hz bus. One is the unfiltered bus voltage, the second is the filtered bus voltage, and the last is the bus current waveform. The harmonic spectrums of these waveforms to be discussed in this section should also be compared with the computer simulation results that were obtained in Part I of this article for the 3Ø/400 Hz bus case. Since both 60 Hz and 400 Hz bus waveforms are synthesized from the 20 kHz HF ac link half cycles the quality of the waveforms obtained in experimental results in terms of their total harmonic distortion (THD) content should even be better than that of the computer simulations because of the much lower frequency of the experimental work compared with that of the simulations.

Fig. 11 shows the harmonic spectrum of the unfiltered line-to-line synthesized bus voltage established with the tight current-regulation technique over a frequency range of 0–100 kHz. This unfiltered bus voltage exists just before the filter inductor and right after the 3Ø PDM converter seen in Fig. 1. The harmonic spectrum is in a logarithmic scale and covers a range of −10 dB to −50 dB. A piece of the waveform whose harmonic content is shown in the above trace is included in the bottom trace of the same figure. Between about 5 kHz and 35 kHz range there is quite a high harmonic content of the waveform reaching to −25 dB. The fundamental component at 60 Hz appears in the −12.5 dB range. At 40 kHz and 80 kHz there are two distinct peaks in the spectrum due to the switching frequency and its multiples. The fact that they seem to appear in slightly less than 40 and 80 kHz is due to the

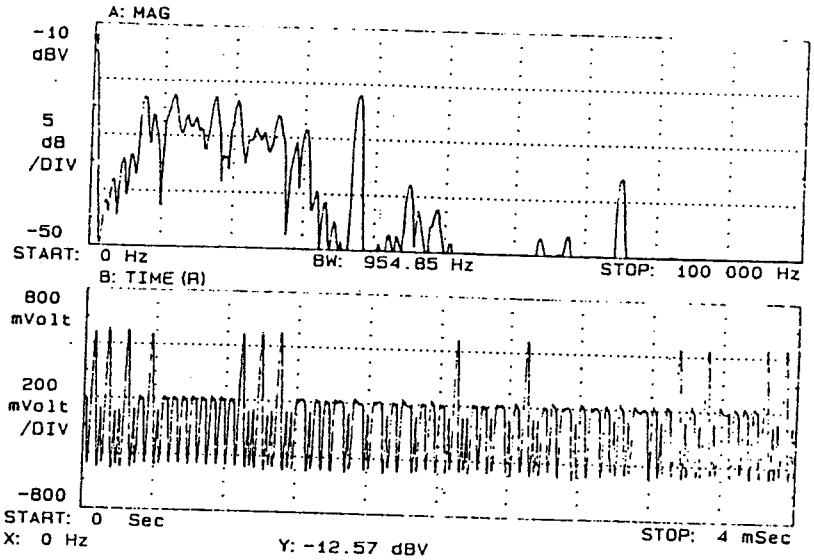

Fig. 11. Top Trace: Phase-AB line-to-line unfiltered synthesized bus voltage (V_{abbus}) harmonic spectrum over 0 to 100 kHz frequency and −50 to −10 dB amplitude range, 10 dB/div, Frequency/div: 10 kHz. Bottom Trace: Phase-AB line-to-line unfiltered synthesized bus voltage, 200 V/div. Time/div: 4 ms.

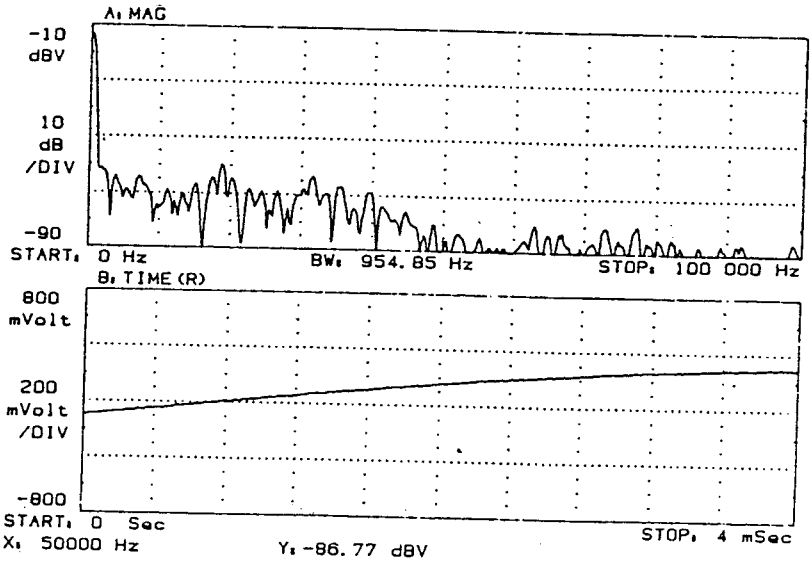

Fig. 12. Top Trace: Phase-AB line-to-line filtered bus voltage (V_{abf}) harmonic spectrum over 0 to 100 kHz frequency and −90 to −10 dB amplitude range, 20 dB/div, Frequency/div: 10kHz. Bottom Trace: Phase-AB line-to-line filtered bus voltage, 100 V/div. Time/div: 4 ms.

fact that the resonant frequency of the resonant tank circuit elements of the HF ac link does not exactly match 20 kHz but rather somewhere around 19 kHz. Therefore the basic converter switching frequency is around 38 kHz. Although the THD of this experimental waveform was not measured, one can have a rough idea from the waveforms obtained in Part I. The computer simulations run for a 400 Hz fundamental frequency had revealed that the unfiltered bus voltage waveforms had THDs slightly higher than 30%. Since the experimental waveforms are realized with 60 Hz fundamental frequeny the THD should be a somewhat lower than 30%. It is worth noting here that the THD definition used here is the rms of all harmonics but the fundamental divided by the total rms value of the waveform.

Fig. 12 shows the improvement in the quality of the bus voltage waveform after the filtering. The harmonic spectrum of the filtered bus voltage is over the frequency range of 0–100 kHz and logarithmic scale of −10 to −90 dB. When this figure is compared with that of the unfiltered bus voltage spectrum over the same frequency range, a drastic improvement can be observed. There is almost no component of the filtered bus voltage other than the fundamental component over −60 dB whereas the unfiltered waveform had components reaching as high as −22 dB. The smooth sine wave

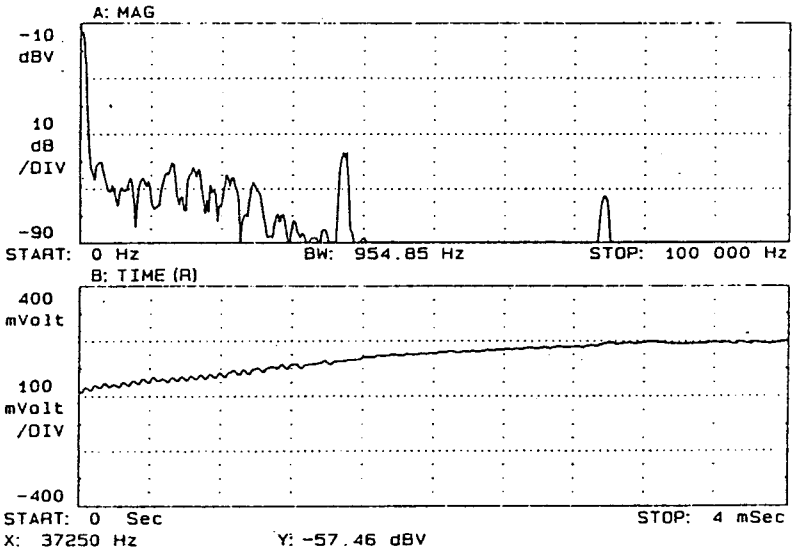

Fig. 13. Top Trace: Phase-A bus line current (i_{abus}) harmonic spectrum over 0 to 100 kHz frequency and −90 to −10 dB amplitude range, 20 dB/div, frequency/div: 10 kHz. Bottom Trace: Phase-A bus line current, 20 A/div. Time/div: 4 ms.

shape of the filtered bus voltage can be observed in the bottom trace of Fig. 12 as opposed to the unfiltered waveform observed in the bottom trace of Fig. 11. Even though the THD of this wavefrom is not measured experimentally, it is estimated that it is even lower than what is found in computer simulation results of Part I of this article because of the lower fundamental frequency. Therefore, THDs of around 1% or less for the filtered bus voltage waveforms are estimated for the experimentally obtained waveforms.

Fig. 13 shows the bus current waveform harmonic spectrum during loaded operation of the bus over a frequency range of 0–100 kHz and logarithmic scale range of −10 to −90 dB. There are some harmonics between the fundamental and 25 kHz which do not exceed −60 dB. Around the switching frequency of 38 kHz, a peak of −42 dB occurs and at twice the switching frequency another peak of less than −70 dB is observed. A piece of the bus current waveform whose harmonic spectrum is shown in the upper trace is shown in the bottom trace. Overall, the bus current waveform looks quite clean. With the computer simulation results for 400 Hz at hand the THD for the experimental 60 Hz bus current waveforms were estimated to be less than 5% under load.

VIII. CONCLUSIONS

The feasibility of a new procedure to start a JE and generating power using a single IM has been shown by means of a hardware prototype. A 3Ø/60 Hz, 115 V line-to-line rms bus waveform independent of the generator speed is established and maintained experimentally. The 60 Hz is chosen for the experimental phase as opposed to the 400 Hz of software simulation phase because of the synchronization studies of the established bus with the existing 60 Hz utility in the laboratory. A 400 Hz experimental operation would require about 7 times bigger filter capacitor as opposed to 60 Hz operation. The phase difference between the reference and the filtered bus voltages faced at 60 Hz operation due to the bang-bang current-regulation technique would be more prevalent for 400 Hz operation. This phase difference might be further reduced by utilizing an hysteresis or other smart current-regulation techniques.

The system investigated here is unique in that it can also be classified as a variable speed constant frequency (VSCF) three-phase power supply employing an induction generator (IG). The IG which would be driven by a JE turbine in the original application may acquire variable speeds and need not be regulated during its operation while it is maintaining operation of the 3Ø/400 Hz bus.

APPENDIX A

Name Plate Ratings of the IM:

3Ø, 60 Hz, 30 Hp, 230/460 V, 68.4/34.2 A, 3545 r/min.

Equivalent Circuit Parameters for 230 V, 68.4 A *Connection*:

$$r_{1dc} = 0.041369\ \Omega, \qquad r_2 = 0.03090\ \Omega,$$

$$r_M = 58.46\ \Omega, \qquad L_{l1} = L_{l2} = 0.4278\ \text{mH},$$

$$L_M = 17.404\ \text{mH}, \qquad s_R = 0.015277.$$

Field-Oriented Controller Settings for 230 V, 68.4 A *Connection*:

$$i_{dsrated} = 27.871\ \text{A peak}, \qquad i_{qsrated} = 92.627\ \text{A peak},$$

$$i_{dsrated} = 19.707\ \text{A rms}, \qquad i_{qsrated} = 65.497\ \text{A rms},$$

$$s_R\omega_e = 5.7593\ \text{rad/s}.$$

APPENDIX B

Name Plate Ratings of the DC Machine:

30 Hp Absorb, 250 V, 82 A, 1700–3600 r/min.

Equivalent Circuit Parameters:

$$\Sigma r_{dc} = 0.3833\ \Omega.$$

REFERENCES

[1] Maldonado, M. A., Shah, N. M., Kleek, K. J., Walia, P. S., and Korba, G. J. (1997)
Power management and distribution system for a more electric aircraft (MADMEL)—Program status.
In *Proceedings of the 1997 Intersociety Energy Conversion Engineering Conference* (IECEC'97), **1** (1997), 274–279.

[2] Maldonado, M. A., Shah, N. M., Kleek, K. J., Walia, P. S., Korba, G. J. (1996)
Power management and distribution system for a more electric aircraft (MADMEL)—Program status.
In *Proceedings of the IECEC'96*, **1** (1996), 148–153.

[3] Homeyer, W. G., Bowless, E. E., Lupan, S. P., Walia, P. S., Maldonado, M. A. (1997)
Advanced power converters for more electric aircraft applications.
In *Proceedings of the IECEC'97*, **1** (1997), 591–596.

[4] Cloyd, J. S. (1997)
A status of the United States Air Force's more electric aircaft initiative.
In *Proceedings of the IECEC'97*, **1** (1997), 681–686.

[5] Homeyer, W. G., Bowless, E. E., Lupan, S. P., Rodriguez, C., Walia, P. S., Shah, N. M., Maldonado, M. A. (1996)
Advanced power converters for more electric aircraft applications.
In *Proceedings of the IECEC'96*, **1** (1996), 137–142.

[6] Fronista, G. L., and Bradbury, G. (1997)
An electromechanical actuator for a transport aircraft spoiler surface.
In *Proceedings of the IECEC'97*, **1** (1997), 694–698.

[7] Elbuluk, M. E., and Kankam, M. D. (1996)
Potential starter/generator technologies for future aerospace application.
IEEE Aerospace and Electronics Systems Magazine, **11**, 10 (1996), 17–24.

[8] Elbuluk, M., and Kankam, M. D. (1995)
Motor drive technologies for the power-by-wire program, Part I—Motors and controllers.
IEEE Aerospace and Electronics Magazine (Nov. 1995), 37–42.

[9] Elbuluk, M., and Kankam, M. D. (1995)
Motor drive technologies for the power-by-wire program, Part II—Power electronic converters and devices.
IEEE Aerospace and Electronics Magazine, (Dec. 1995), 31–36.

[10] Skvarenina, T. L., Pekarek, S., Wasynczuk, O., Krause, P. C., Thibodeaux, R. J., and Weimer, J. (1997)
Simulation of a switched reluctance, more electric aircraft power system using a graphical user interface.
In *Proceedings of the IECEC'97*, **1** (1997), 580–584.

[11] Skvarenina, T. L., Wasynczuk, O., Krause, P. C., Chen, W. Z., Thibodeaux, R. J., and Weimer, J. (1996)
Simulation and analysis of a switched reluctance generator/more electric aircraft power system.
In *Proceedings of the IECEC 96*, **1** (1996), 143–147.

[12] Radun, A. V., and Jiang, H. (1995)
400 Hz ac generator/cycloconverter using switched reluctance technology for aircraft retrofit/upgrade applications.
WPAF contract report, Apr. 1995.

[13] Ferreira, C., Johns, S. R., Heglund, W. S., and Johns, W. D. (1995)
Detailed design of a 30-kW switched reluctance starter/generator system for gas turbine engine application.
IEEE Transactions on Industry Applications, **31**, 3 (May/June 1995), 553–561.

[14] Ferreira, C. A., Johns, S. R., and Heglund, W. S. (1995)
Performance evaluation of a switched reluctance starter/generator system under constant power and capacitive type loads.
IEEE Transactions on Industry Applications, **31**, 3 (May/June 1995), 553–561.

[15] Heglund, W. S., Drager, B. T., Johns, S. R., and Ferreira, C. A. (1995)
Design and implementation of a five-hp, switched reluctance, fuel lube, pump motor drive for gas turbine engine.
IEEE Transactions on Power Electronics, **10**, 1 (Jan. 1995), 55–61.

[16] Johns, S. R., and Drager, B. T. (1995)
Performance evaluation of a high speed switched reluctance starter/generator system using electronic position sensing.
In *Proceedings of the IEEE IAS'95*, 249–253.

[17] Richter, E., and Ferreira, C. (1995)
Performance evaluation of a 250 kW switched reluctance starter/generator.
In *Proceedings of the IEEE IAS'95*, 434–440.

[18] Rim, G., and Krishnan, R. (1994)
Variable speed constant frequency power conversion with a switched reluctance machine.
In *Proceedings of the IEEE APEC'94*, 63–71.

[19] Radun, A., Ferreira, C., and Richter, E. (1998)
Two-channel switched reluctance starter/generator results.
IEEE Transactions on Industry Applications, **34**, 5 (1998), 1026–1034.

[20] Radun, A. V. (1994)
Generating with the switched reluctance motor.
In *Conference Proceedings of the APEC'94*, Feb. 13–17, 1994, 41–47.

[21] Radun, A. V., Lyons, J. P., Ruison, J., Sanza, P., Richter, E. (1994)
Engine starter/generator system testing.
Aerospace Engineering (July 1994), 23–26.

[22] Richter, E., Lyons, J. P., Ferreira, C., Radun, A. V., and Ruchstadter, E. (1994)
Starter generator preliminary testing of a 250 kW reveals favorable results.
Aerospace Engineering (Oct. 1994), 7–10.

[23] Radun, A. V. (1992)
High power density switched reluctance motor drive for aerospace power applications.
IEEE Transactions on Industry Applications, **28**, 1 (Jan./Feb. 1992), 113–119.

[24] MacMinn, S. R., and Sember, J. W. (1989)
Control of a switched-reluctance aircraft engine starter/generator over a very wide speed range.
In *Proceedings of the IECEC'89*, 631–638.

[25] MacMinn, S. K., and Jones, W. D. (1989)
A very high speed switched-reluctance starter generator for aircraft engine applications.
In *Proceedings of NAECON'89*, Dayton, OH, May 22–26, 1989, 1758–1764.

[26] Jahns, T. M., and Maldonado, M. A. (1993)
A new resonant link aircraft power generating system.
IEEE Transactions on Aerospace and Electronic Systems, **29** (Jan. 1993), 206–214.

[27] Jahns, T. M., DeDoncker, R. W., Radun, A. V., Szczesny, P. M., Turnbull, F. G. (1993)
System design considerations for a high power aerospace resonant link converter.
IEEE Transactions on Power Electronics, **8**, 4 (Oct. 1993), 663–672.

[28] Lipo, T. A., and Sood, P. K. (1986)
Feasibility study of an induction generator system employing a bi-directional resonant converter for aircraft power supply.
Final report, NASA Grant NAG3-492, Apr. 4, 1986.

[29] Lipo, T. A., and Sood, P. K. (1987)
Study of the generator/motor operation of induction machine in a high frequency link space power system.
NASA Contractor Report, contract NAG 631, Mar. 1987.

[30] Lipo, T. A., and Sul, S. K. (1988)
Design and test of bidirectional speed and torque control of induction machines operating from high frequency link converter.
Final report, NASA contract NAG3-786 (Apr. 1988).

[31] Sood, P. K., and Lipo, T. A. (1988)
Power conversion distribution system using a resonant high-frequency AC link.
IEEE Transactions on Industry Applications, **24** (Mar./Apr. 1988), 288–300.

[32] Sood, P. K., Lipo, T. A., and Hansen, I. (1988)
A versatile power converter for high frequency link systems.
IEEE Transactions on Power Electronics, **3**, 4 (Oct. 1988), 383–390.

[33] Sul, S. K., and Lipo, T. A. (1990)
Design and performance of a high frequency link induction motor drive operating at unity power factor.
IEEE Transactions on Industry Applications, **26**, 3 (May–June 1990), 434–440.

[34] Sul, S. K., and Lipo, T. A. (1990)
Field oriented control of an induction machine in a high frequency link power system.
IEEE Transactions on Power Electronics, **5**, 4 (Oct. 1990), 436–445.

[35] Lipo, T. A., Sul, S. K., and Alan, I. (1988)
Testing and modification of the general dynamics converter.
NASA Interim Report, contract NAG3-786, Eylül, 1988.

[36] Sul, S. K., Alan, I., and Lipo T. A. (1989)
Performance testing of a high frequency link converter for space station power distribution system.
In *Proceedings of 1989 Intersociety Energy Conversion Engineering Conference*, Washington, DC, Aug. 1989, Vol. 1, *Aerospace Power Systems and Power Conditioning*, 617–624.

[37] Lipo, T. A., and Alan, I. (1991)
System and component design and test of a 10 hp, 18,000 rpm AC dynamometer utilizing a high frequency AC voltage link.
Final report, contract NAG3-940, June 1991.

[38] Lipo, T. A., and Alan, I. (1992)
Design and test of a flywheel load leveling system utilizing a 20 kHz parallel resonant HF ac voltage link.
NASA final contractor report, contract NAG3-1299, June 1992.

[39] Alan, I. (1993)
A completely isolated 3-phase to 3-phase induction motor/induction generator power conversion system.
Ph.D. dissertation, University of Wisconsin–Madison, Dec. 1993.

[40] Alan, I., and Lipo, T. A. (1994)
Control of polyphase induction generator/induction motor power conversion system completely isolated from the utility.
IEEE Transactions on Industry Applications, **30**, 3 (May–June 1994), 636–647.

[41] Alan, I., and Lipo, T. A. (1995)
Feasibility study of a battery started induction generator maintained 3-phase/400 Hz voltage regulated bus utilizing high frequency ac link.
Final report, contract NAG3-1447, May 1995.

[42] De Doncker, R. D., and Lyons, J. P. (1991)
Control of three phase power supplies for ultra low THD.
In *Proceedings of 6th Annual Applied Power Electronics Conference and Exposition*, APEC 91, 622–629.

[43] Vaidya, J. G. (1991)
Electrical machines technology for aerospace power generator.
Proceedings of IECEC 1991, **1** (1991), 7–12.

[44] Brune, C. S., Spee, R., and Wallace, A. K. (1994)
Experimental evaluation of a variable speed, doubly-fed wind-power generation system.
IEEE Transactions on Industry Applications, **30**, 3 (May/June 1994), 648–655.

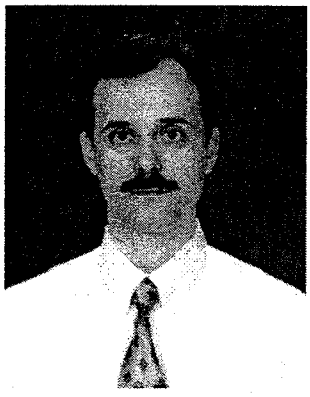

Irfan Alan (S'91—M'94) was born in Istanbul, Turkey. He received the B.E.E. and M.S.E.E. degrees from the Istanbul Technical University (ITU) in 1983 and 1986 respectively, and the Ph.D. degree in electrical engineering from the University of Wisconsin–Madison in 1993.

He was appointed a Research Assistantship during his M.S. studies at ITU. During most of his Ph.D. studies he was a research assistant at UW–Madison, working on various NASA projetcs. During his post doctorate studies at UW–Madison he was a research associate and worked on another NASA project. He was employed as a project officer at NATO Headquarters Command in Izmir-Turkey during his compulsory military service in 1996–1997. Since then he had been an Assistant Professor at Ege University in Izmir, Turkey. He is the Associate Chairman of the Electrical Engineering Department of Ege University Engineering Faculty since 1997, Chairman of Electrical Machine Branch, and an Associate Professor since November 1998. His research interests are in solid state power conversion systems and ac machine drives in general, and resonant and matrix power converters and drives in particular.

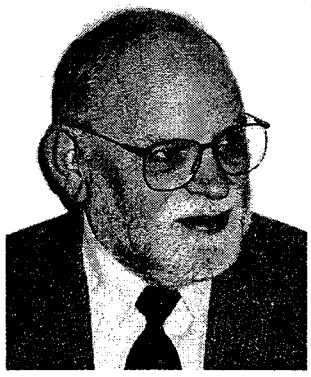

Thomas A. Lipo (M'64—SM'71—F'82) was born in Milwaukee, WI. He received the B.E.E. and M.S.E.E. degrees from Marquette University, Milwaukee, WI in 1962 and 1964, and the Ph.D. degree in electrical engineering from the University of Wisconsin, Madison, in 1968.

From 1969 to 1979, he was an Electrical Engineer in the Power Electronics Laboratory of Cooperate Research and Development of the General Electric Company, Schenectady, NY.

He became Professor of Electrical Engineering at Purdue University, West Lafayette, IN, in 1979, and in 1981 he joined the University of Wisconsin, Madison, in the same capacity, where he is presently the W. W. Grainger Professor for Power Electronics and Electrical Machines.

Dr. Lipo received the Outstanding Achievement Award from the IEEE Industry Applications Society, William E. Newell Award of the IEEE Power Electronics, and the 1995 Nicola Tesla IEEE Field Award from the Power Engineering Society for his work. He has served IEEE in various capacities, including President of the Industrial Applications Society.